TECHNICAL PAPER

Effect of specimen size and shape on the compressive performance of high strength engineered cementitious composites at elevated temperatures

S. Rawat[1,2] · Y. X. Zhang[1] · C. K. Lee[2]

Abstract

This study provides detailed insights into the effect of specimen size on the residual compressive strength of hybrid polyethylene-steel fibre reinforced high strength engineered cementitious composite after exposure to elevated temperatures. A mix design with high residual performance was selected and a total of 120 specimens with different cross-section shape (square and circular), aspect ratio (1 and 2) and sizes (cylinders of 40 mm, 75 mm, 100 mm, 150 mm diameter with height to diameter ratio of 2:1, cubes of 50 mm, 75 mm, 100 mm side and prism of size $75 \times 75 \times 150$ mm) were cast. These specimens were subjected to temperatures ranging from 200 to 800 °C and the residual compressive strength and change in microstructure was then analysed after air cooling. Experimental results indicated that cubic specimens experienced less strength loss compared to prism specimens with the same cross-sectional area and the damage was found to decrease with increase in the volume to surface area ratio of the specimens. Furthermore, no spalling occurred in any of the specimens despite the change in specimen size or cross-section. Unlike previous studies that did not present any clear influence of specimen size, the present work established that the residual strength is dependent on aspect ratio and volume to surface area ratio of the specimen. As a result, these findings are valuable for selecting appropriate specimen size in elevated temperature studies and for the development of suitable guidelines to facilitate meaningful comparisons with the existing data.

Introduction

Engineered cementitious composite (ECC) is a special type of fibre reinforced cementitious composite, micromechanically designed to exhibit high tensile ductility and enhanced durability [1]. Despite its improved properties, ECC is susceptible to fire hazard due to its dense and compact microstructure. To address this issue, use of various of types of polymer, metallic or natural fibres have been assessed and low melting point polymer fibres such as polypropylene (PP), linear low-density polythene (LLDPE), and polyvinyl alcohol (PVA) have proven to be particularly efficient in preventing spalling during fire exposure [2]. These fibres melt and vaporize under high temperatures, creating an interconnected network of vacant channels. This network improves the dissipation of pore pressure, thereby enhancing resistance to spalling and overall mechanical performance.

However, it should be noted that the formation of the interconnected network and risk of spalling is greatly dependent on the specimen size. It is easier for the moisture to escape in a smaller sized specimen due to shorter path. Therefore, smaller sized specimens may have better spalling resistance and residual performance when compared to the larger sized specimens [3]. Additionally, this phenomenon might be intensified by the 'size effect' observed during uniaxial compression testing. It is well established that the likelihood of encountering a critical-sized crack increases with the number of cracks i.e., volume of the specimen [4]. Therefore, the combined influence of formation of vacant channels and critical-sized cracks may have a significant impact on the post-exposure compressive performance.

✉ S. Rawat
s.rawat@westernsydney.edu.au

1   School of Engineering, Design and Built Environment, Western Sydney University, Penrith, NSW 2751, Australia

2   School of Engineering and Technology, The University of New South Wales, Canberra, ACT 2600, Australia

Existing studies on ECC utilizes a wide range of specimen sizes to assess the elevated temperature performance and spalling resistance, making it challenging to make justified comparisons among the existing data and predict the actual fire resistance. The magnitude of this variability is highlighted by examining the specimen sizes employed within the last five years, as listed in Table 1. It can be observed that not only there is a significant variation in the size of the specimens, the shape and aspect ratio of the specimens also differs which makes it hard to provide a valid comparison of the existing data. Therefore. it is important to define a coherent link between specimen size and its impact before establishing fire test guidelines for fibre reinforced cementitious composites (FRCC).

In order to address this issue, various researchers have studied the effect of specimen size on the elevated temperature compressive performance of FRCC. Zheng et al. [28, 29] reported that the residual compressive strength tested on 70.7 mm cubic steel fibre reinforced specimens was higher than that tested on the prism ($70.7 \times 70.7 \times 220$ mm). For instance, the residual compressive strength at 400 °C retained by approximately 76% for cubic specimens with 3% (by volume) steel fibres, whereas the retention was just 16% for the prism specimens. Bamonte and Gambarova [30] analysed the size effect in PP-FRCC and also observed relatively higher strength in 40 mm cubic specimens as compared to 36 mm diameter × 110 mm height cylinders. In both studies, larger sized specimens suffered higher loss which may have been due to the delay in formation of interconnected network. On the other hand, Akca and Zihnioglu [31] found better compressive performance in 100 mm cubic specimens as compared to $100 \times 100 \times 50$ mm specimens. 100 mm cubic specimens retained around 60% compressive strength at 600 °C, whereas the retention for the specimens with 50 mm height was 54%. They concluded that the specimens with smaller size could result in higher loss due to rapid heating. Contrary to these findings, Erdem [3] reported

that the residual compressive strength was unaffected by the change in the size of specimens. Cylinder specimens with diameter 50 mm, 100 mm, 150 mm, and height to diameter ratio 2:1 showed similar crack pattern and the influence of elevated temperature on residual compressive strength was also similar with roughly equivalent retention observed until 800 °C. The conflicting findings from these studies highlight a lack of clear correlation between specimen size and performance under elevated temperatures. Consequently, a comprehensive analysis is required to better understand the effect of temperature on different sized specimens, enabling future studies to provide meaningful comparisons with existing data.

Therefore, the main objective of this paper is to extensively investigate how specimen size and shape influence the residual compressive strength of high strength ECC (HSECC). In the authors' previous work, a binary blend of ground granulated blast furnace slag (GGBFS) and cement with GGBFS: cement = 1:1 with hybrid polyethylene (PE)-steel fibre was found to have a superior spalling resistance and residual compressive performance [6, 20]. Consequently, the same mix has been employed in the present study to analyse the residual compressive strength and provide a thorough explanation of the effect of temperature on different sized specimens. Microstructure characterization techniques including scanning electron microscopy (SEM), and X-ray diffraction (XRD) are further utilized to analyse the influence of size at different temperature range. Following a careful and thorough comparison, the variation in the performance of different sized specimen is correlated and a clear effect of specimen size and shape on residual strength has been presented.

Experimental program

Raw materials

ECC mix with cement to GGBFS ratio of 1:1 was used in this study. Details of the mix design are given in Table 2. The main binder materials in the matrix were general purpose cement (specific gravity 3.15 and fineness 350 m^2/kg) and GGBFS (specific gravity 2.91 and fineness 445 m^2/kg). Their chemical compositions are further outlined in Table 3. The aggregate used was oven-dried sand, passing through 300 microns with average particle diameter of 200 microns. In addition to this, water and high range water reducer (HRWR) were used as a solution to ensure sufficient flowability of the mix. HRWR was poly-carboxylic ether type with brand name ADVA650 and it was procured from GCP Applied Technologies, Australia. Additionally, hybrid combination of PE and steel fibre was also used to impart better spalling resistance and residual performance as

Table 1 Specimen size used in existing studies for residual compressive performance analysis

| Specimen type	Specimen size	References (year 2019–2024)
Cube	40 mm	[5]
	50 mm	[6–10]
	70.7 mm	[11, 12]
	100 mm	[13–15]
Cylinder	50 mm diameter × 100 mm height	[16, 17]
	75 mm diameter × 150 mm height	[18–20]
	100 mm diameter × 200 mm height	[21–24]
Prism	40 mm × 40 mm × 80 mm	[25]
	40 mm × 40 mm × 160 mm	[11, 26, 27]

Table 2 Mix proportions used in this study

Cement (kg/m^3)	GGBFS (kg/m^3)	Sand (kg/m^3)	Water (kg/m^3)	HRWR (Lit/m^3)	PE fibre (% vol)	Steel fibre (% vo)
636	636	462	254.4	24.56	1.5%	0.75%

Table 3 Chemical composition of the binder material

Element	CaO	SiO$_2$	Al$_2$O$_3$	Fe$_2$O$_3$	MgO	Na$_2$O	K$_2$O	SO$_3$	Loss on ignition
Cement	63.74	18.51	5.11	2.92	0.92	0.13	0.36	2.64	4.97
GGBFS	41.25	34.38	13.31	0.71	4.75	0.35	0.28	2.85	<0.01

Table 4 Properties of the fibre used

Fibre type	Density (gm/cm^3)	Tensile strength (MPa)	Young's modulus (GPa)	Diameter (μm)	Length (mm)	Aspect ratio
PE	0.97–0.98	3000	116	24	12	500
Steel	7.8	>2200	200	200	13	65
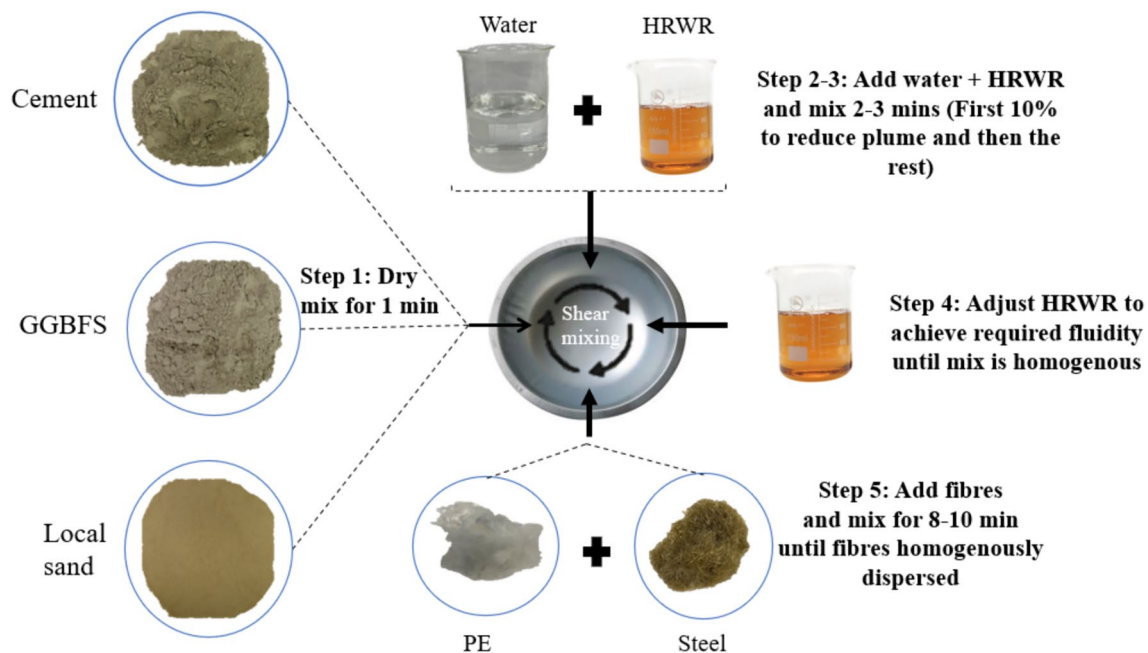
Fig. 1 Mixing procedure of HSECC

recommended in authors' previous work [6, 20, 32]. Further details on the properties of fibres are presented in Table 4.

Specimen preparation and curing

The mixing was done in a 100-litre mixer with rotating shaft as per the procedure illustrated in Fig. 1. Firstly, the sand was poured in the mixer along with other binder material and mixed for around 1 min. Approximately 10% of the water + HRWR solution was added initially to reduce the plume. After the dry mixing, the remaining water + HRWR solution was added, and the mixing continued for 2–3 min. Additional HRWR was adjusted based on flowability requirements to achieve a homogeneous mix. Subsequently, fibres were gradually added, and mixing continued for 8–10 min until uniform distribution was achieved. Once the mix was prepared, it was transferred directly into each of the greased moulds in a single pour to avoid any layering effect and proper compaction was ensured through the use of a vibration table.

The types of specimens considered are (Fig. 2): cubes of size 50 mm, 75 mm, and 100 mm, 75 mm × 75 mm × 150 mm prism, cylinders of diameter 40 mm, 75 mm, 100 mm, and 150 mm with height to diameter ratio of 2:1. All the different sized specimens were cast in a single batch except the 150 mm diameter × 300 mm height cylinders to eliminate any variation due to mixing. Cylinders of 150 mm diameter were cast in three batches due to the limited number of moulds available. Nevertheless, for each of the casted

batch, specimens were tested at ambient conditions in order to confirm that their mechanical properties are consistent.

The specimens were demoulded 18–24 h after casting and were placed in fog room for curing for 28 days at 23 ± 1 °C and $95 \pm 5\%$ relative humidity. Thereafter, all the specimens were transferred to 20 ± 1 °C and $55 \pm 5\%$ relative humidity and were kept there for another 28 days. The casting procedure is further illustrated through Fig. 3.

Testing program

After the completion of curing period, all the specimens were exposed to 200, 400, 600, and 800 °C following the heating profile depicted in Fig. 4a. The heating was done at a constant rate of 1 °C/min to avoid unnecessary thermal gradients that could affect the resulting strength. The dwell duration was confirmed by measuring the temperature at the centre and surface of a 150 mm cube when the temperature increased from 20 to 1000 °C. It was observed that approximately 1.3 h were required for the core of the specimens to reach the target temperature (Fig. 4b). Given that the shortest distance from the centroid of the 150 mm cube to any of its sides (75 mm) was equal to or greater than all other specimens tested in this study, a 2-h hold duration was considered adequate to ensure thorough heating of all specimen cores. This duration has also been employed consistently in previous studies [2, 33, 34].

After the completion of the dwelling period, the specimens were allowed to cool down naturally by turning off the furnace. Thereafter, specimens were tested under compression at a displacement rate of 0.05 mm/min. An average was calculated for each temperature range and specimen size by conducting tests on three specimens in each group. This resulted in a total of 120 specimens tested, comprising five temperature ranges, eight different specimen sizes, and three specimens per set. Cube and prism specimens were tested in the direction perpendicular to the casting, whereas cylinder specimens underwent testing parallel to the casting direction.
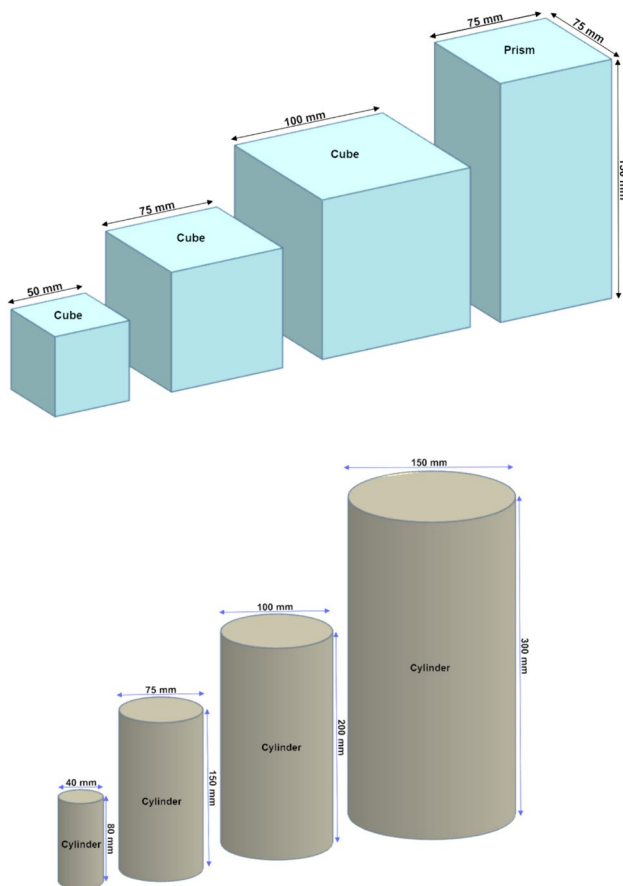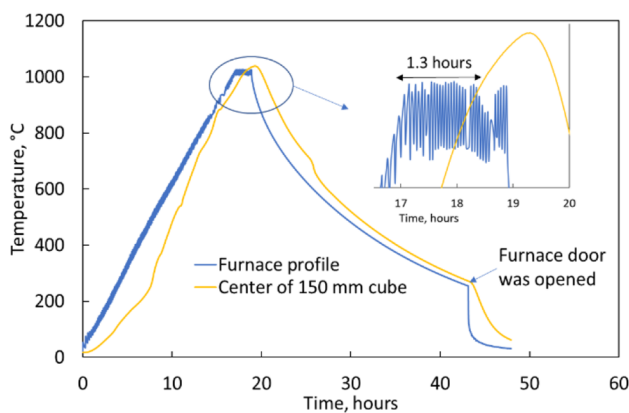

Fig. 2 Types of specimens used in the present study

Fig. 3 Different stages of HSECC casting

(a) Mixing   (b) Compaction   (c) Mould filled with HSECC   (d) Curing in fog room
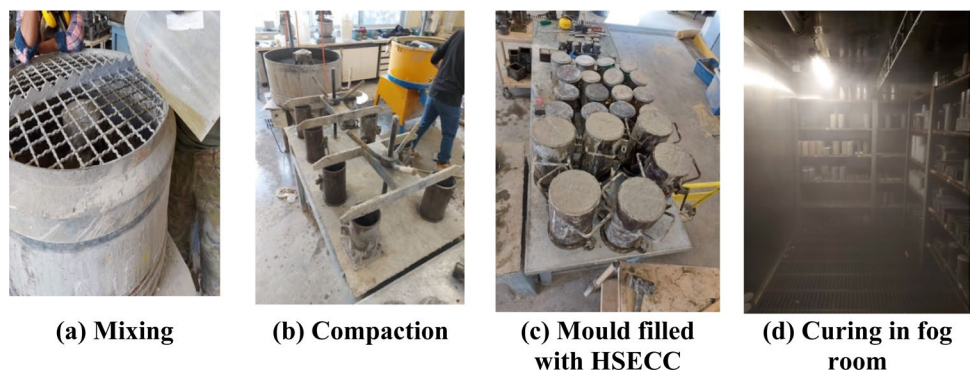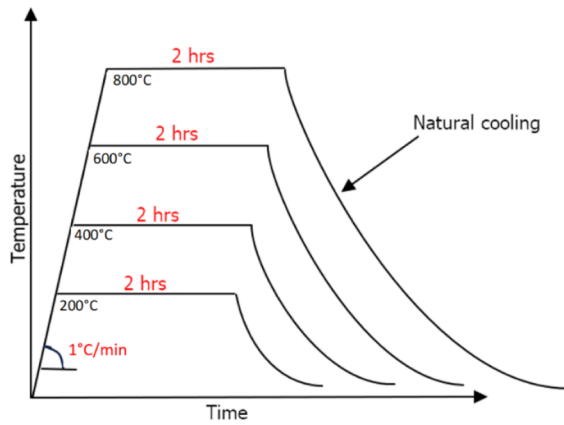
(a) General time-temperature profile

(b) Time-temperature profile for 150 mm cube

Fig. 4 Temperature-time profile used for elevated temperature testing

Following the compression testing, small samples were taken from the core of each HSECC specimen set. These samples were immersed in acetone for a minimum of 48 h to halt further hydration and then dried at 60 °C for an additional 24 h. Subsequently, a portion of the sample, both in solid and powdered form, was utilized for characterisation study to perform SEM and XRD analysis, respectively. For microstructural analysis, solid samples were initially carbon-coated and examined using a Phenom XL SEM operating at 15 kV and 1 Pa chamber pressure. Elemental composition of the samples was further analysed using the Phenom energy dispersive spectroscopy (EDS) system. XRD patterns were obtained using a Bruker D8 Advance XRD system with an accelerating voltage and current of 40 kV and 40 mA, respectively. Powdered samples were mounted in a Bruker back-loading sample holder and scanned from 5° to 80° 2θ, with a step size of 0.02° 2θ and a counting time of 2.5 s per step.

Results and discussions

Qualitative characterisation

Figures 5 and 6 show the colour change in the specimens of square and circular cross-section after exposure to elevated temperatures. It is evident that the colour change is quite similar across all types of specimens. As the temperature increases from 20 to 200 °C, the specimens turn to light-yellow shade, which gradually transitions to white at 800 °C. More importantly, none of the specimens experienced spalling. The general crack pattern was also similar with no observable cracks until reaching 600 °C. However, at 800 °C, more noticeable cracks appeared in the 50 mm cube and 40 mm cylinder specimens. It was likely due to their smaller size within their corresponding series. Since the dwelling duration was kept constant for the heating, it is expected that the smaller sized specimens may have achieved isothermal stage before the large specimens, leading to a longer dwell time at the reference temperature. This extended exposure likely contributed to the increased formation of cracks in these smaller sized specimens.

Effect of specimen size on mass loss

Mass loss at elevated temperature is mainly caused by the loss of free water, absorbed interlayer water and chemically bound water. In addition, the melting of fibre and decomposition of matrix also slightly contributes to this loss [2]. Therefore, it is a relatively direct process primarily influenced by the matrix composition and level of heat exposure. Furthermore, the most substantial loss of mass, attributed mainly to water evaporation, occurs before 400 °C. As a result, the trend in mass loss significantly differs up to this temperature, depending on the extent of exposure.

Specimens with square cross-section

Figure 7 compares the average mass loss of specimens with square cross-section at elevated temperatures. It can be observed that the range of mass loss change is very similar for the size varying from 75 to 100 mm with very small deviation. The average mass loss increased to 6.2–6.9% at 200 °C, showing a steep rise till 400 °C where the mass loss becomes 13.6–14.3%. With further increase in temperature, rate of rise in mass loss decreases, and it only climbs to 15–16% at 800 °C. The 50 mm cube showed an obviously higher mass loss up to 200 °C, after which the rate of mass loss relatively reduced. It is well established that the mass loss rise is very steep until 400 °C due to the evaporation of free water, physically absorbed water, and the interlayer
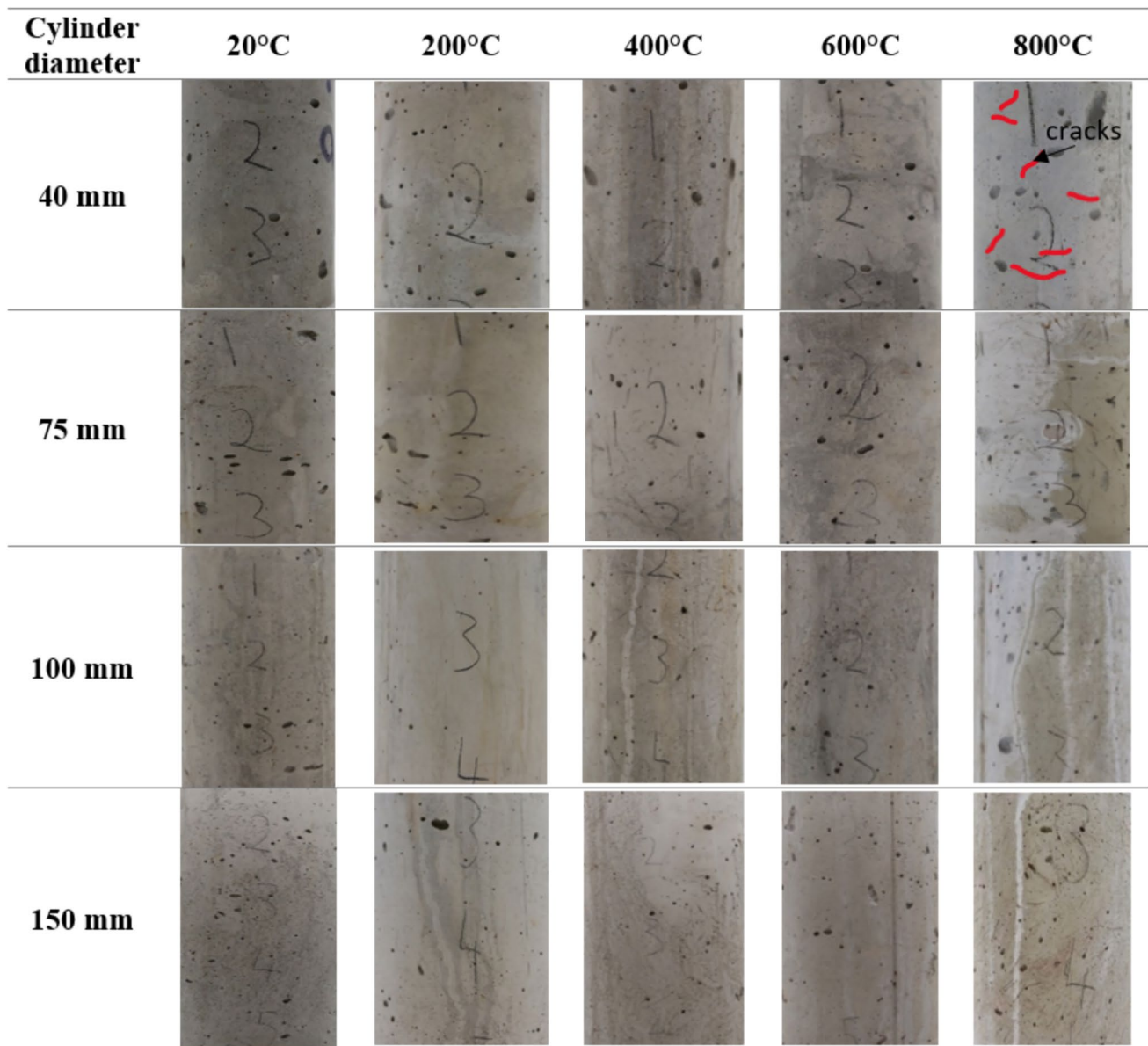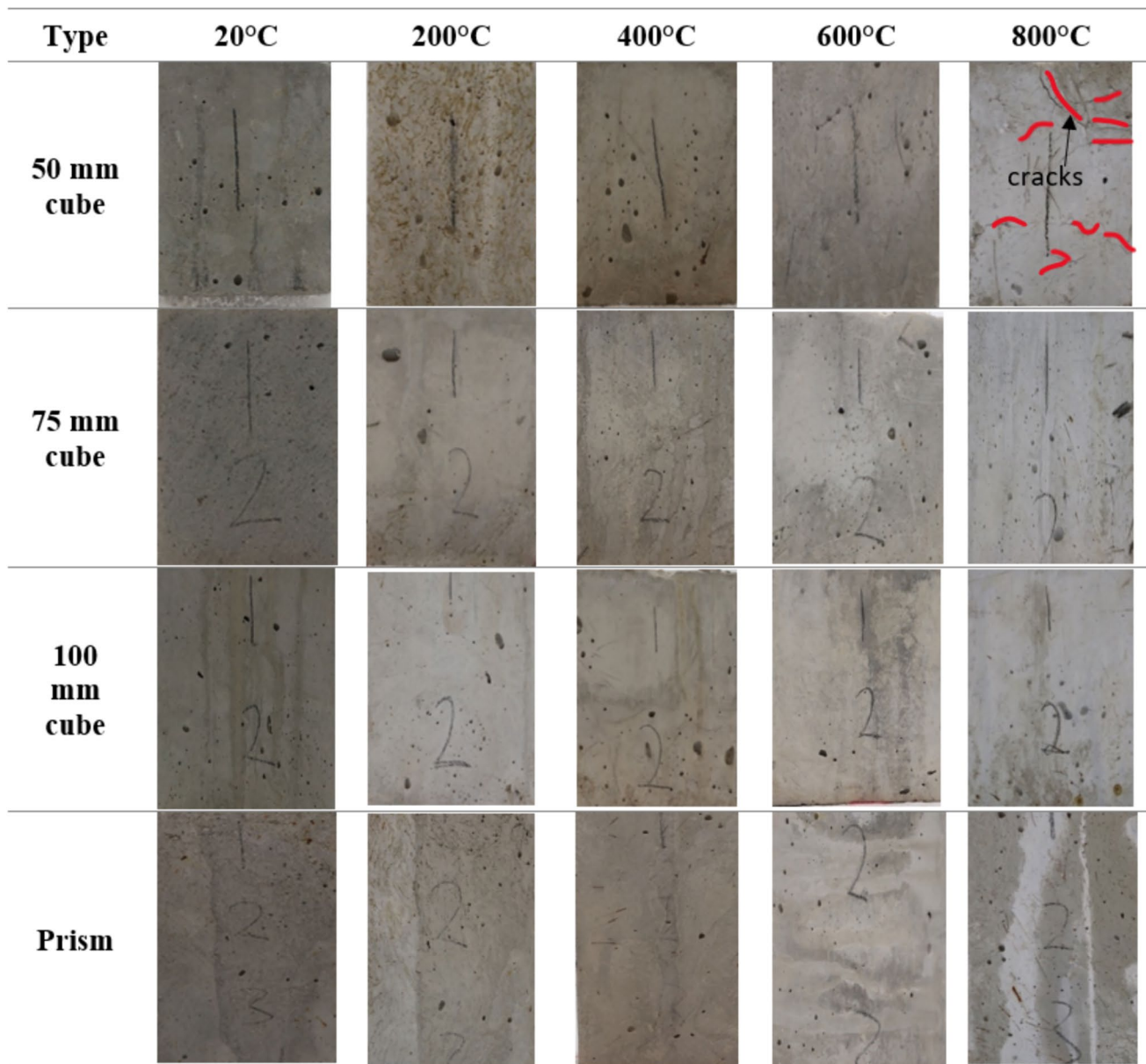
Fig. 5 Surface of specimens with circular cross-section at elevated temperatures

water [2]. The smaller 50 mm cube specimens reached the isothermal state more quickly, potentially staying at that temperature longer, which might have led to more evaporation and consequently greater loss of mass. This likely explains why the 50 mm cubes experienced the highest mass loss, while the 100 mm cubes had the lowest. However, as the temperature increased to 400 °C, where the evaporation of both free and interlayer water nears completion, the rate of mass loss stabilized. After this temperature, the relative difference between the specimens with similar cross-sectional shape but different size was found to be very small. For instance, mass loss observed in 50 mm cube was 13.1%

at 400 °C, whereas it was 13.6% and 13.9% in 75 mm and 100 mm cube respectively.

For the $75 \times 75 \times 150$ mm prims specimens with same cross-section area but higher aspect ratio, the mass loss was similar as cubes until 200 °C as shown in Fig. 8 and the relative rate of mass loss only slightly increased at higher temperature ranges. For instance, mass loss at 800 °C was 15.7% in 75 mm cubic specimens, whereas it was 16% in prism. This slightly higher mass loss could be attributed to factors such as relative distribution of fibres and presence of better interconnected channel network in specimen with higher surface area.

**Fig. 6** Surface of specimens with square cross-section at elevated temperatures

Specimens with circular cross-section

The mass loss in specimens with circular cross-section also followed a similar trend as square cross-section specimen (Fig. 9). The mass loss among cylinders of diameters ranging from 75 to 150 mm was in a comparable range, with values between 6.1–7.5% at 200 °C, increasing to 15.9–16.9% at 800 °C. An exception was noted in the smaller 40 mm cylinder specimens at 200 °C, which exhibited higher mass loss, consistent with observations for 50 mm cubic specimens. The smaller 40 mm cylinder specimens reached the isothermal state more quickly, potentially prolonging their exposure and resulting in greater evaporation and subsequent mass loss. This further explains why the 40 mm cylinders experienced the highest mass loss, while the 100 mm cylinders showed the lowest. Moreover, 150 mm cylinder specimen suffered lower mass loss than 100 mm cylinder specimens at 400 °C, the reason for which is not particularly clear. It may have been due to variation in fibre distribution or different evaporation rate. Further research is required to corroborate this. After 400 °C, the trend of mass loss became consistent, and it marginally increased with increase in specimen size.

Additionally, prism specimens also experienced a slightly higher mass loss than 75 mm cylinder specimens with same aspect ratio as shown in Fig. 10. This may have again been due to the simultaneous exposure of higher surface area in

Fig. 7 Average mass loss in HSECC specimens with square cross section
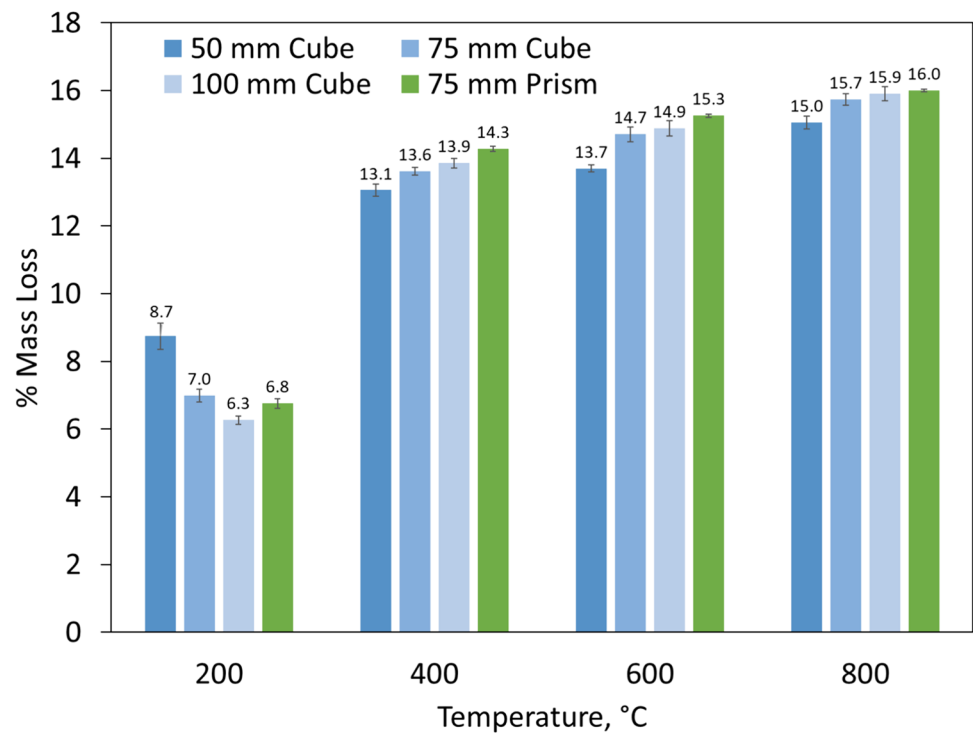
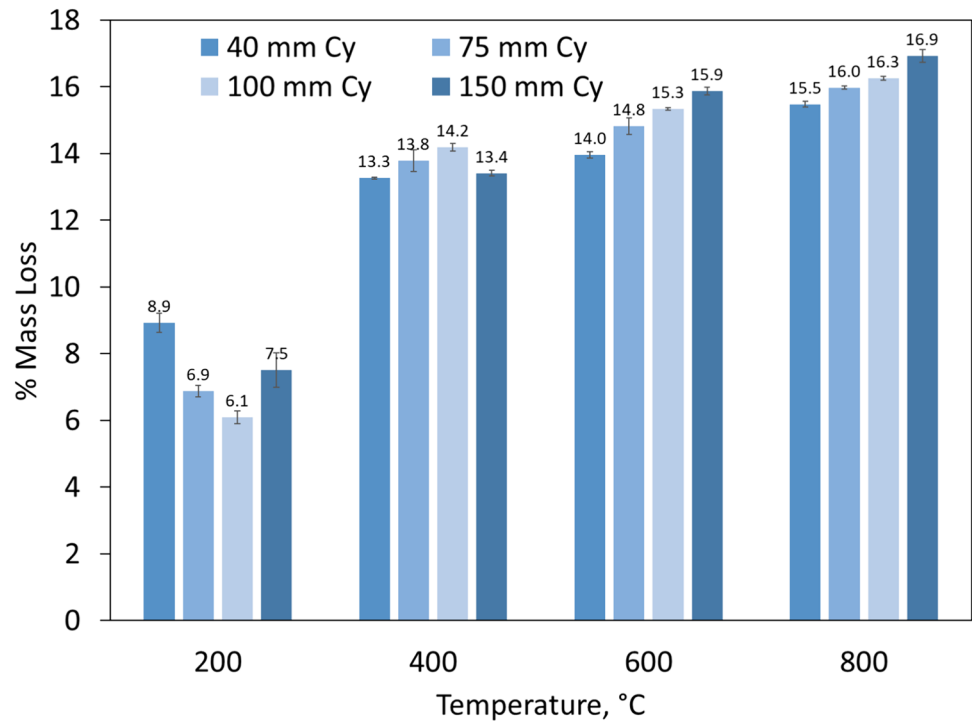**Fig. 8** Comparison of average mass loss between 75 mm cube and 75 mm prism
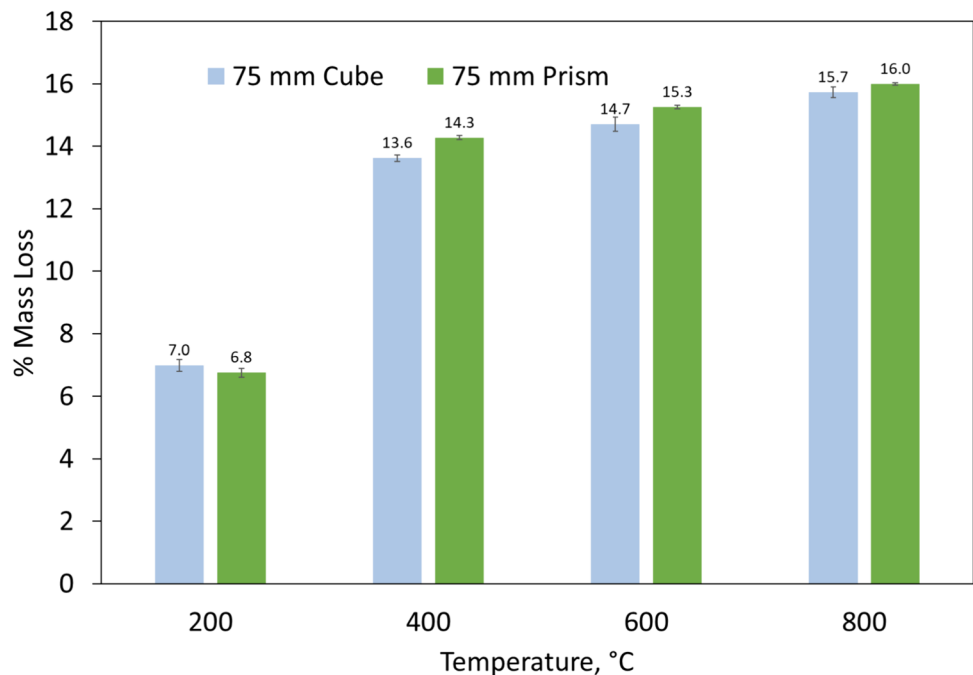
case of prisms (prism surface area = 56,250 mm^2 vs. 75 mm cylinder surface area = 44178.64 mm^2) leading to higher dehydration, and consequently, higher mass loss.

In general, it is evident that change in specimen size has minimal effect on mass loss. The variation is likely to occur at temperatures below 400 °C. This is because of the fact that mass loss is mainly contributed by the evaporation

of free and chemical bound water which predominantly occurs prior to reaching this temperature. Additionally, the formation of interconnected channels typically does not complete before this point due to the higher vaporisation point of PE fibres [32]. Therefore, the degree of evaporation may differ based on the duration of exposure, potentially affecting smaller specimens differently. However,

Fig. 9 Average mass loss in HSECC specimens with circular cross section

**Fig. 10** Comparison of average mass loss between 75 mm cylinder and 75 mm prism
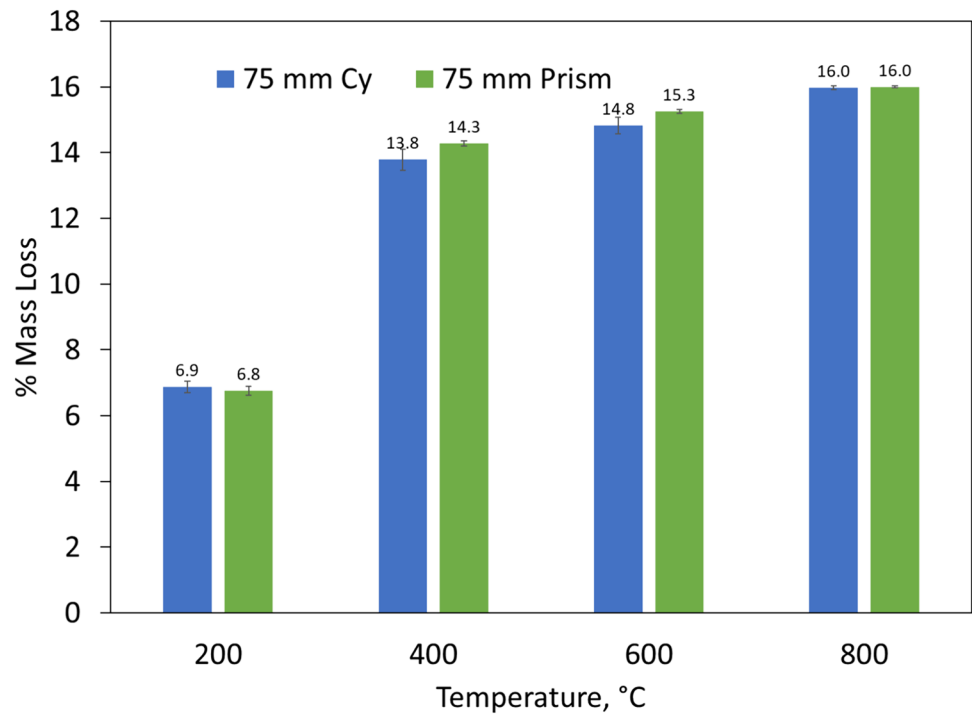
beyond 400 °C, the impact of exposure duration becomes less distinct [35] and hence, the time to reach the isothermal state has very little influence on the total mass loss as evident from the obtained results.

Effect of specimen size on compressive strength

Ambient compressive strength

Figure 11 illustrates the compressive strength of different sized specimens at room temperature. It can be observed that

Fig. 11 Average compressive strength of different sized specimens at ambient temperature
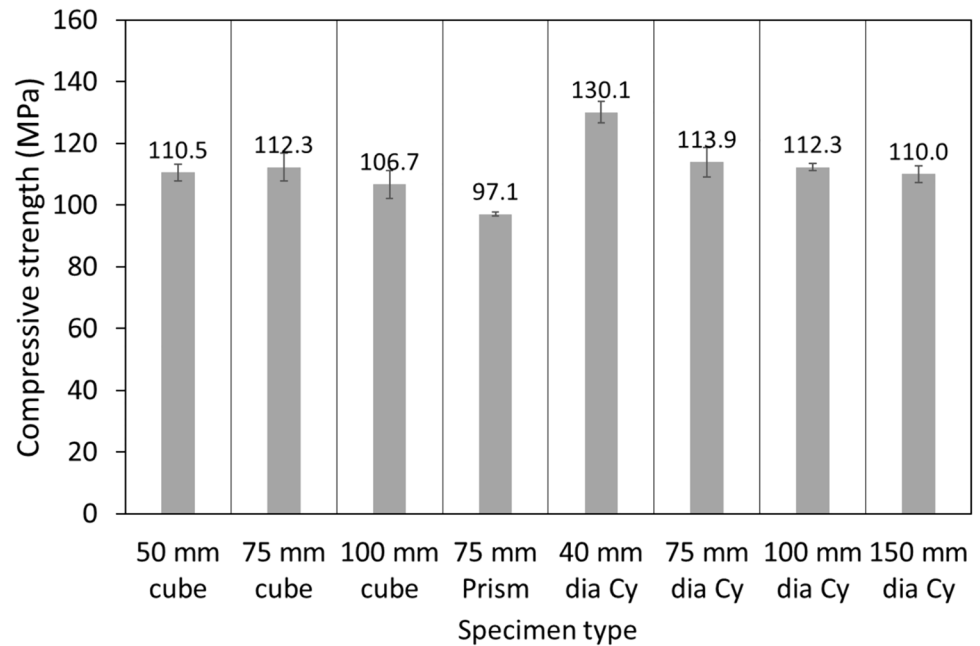

for the square cross-section size varying from 50 to 100 mm, compressive strength varied from 97 to 112 MPa with 75 mm prism showing the least compressive strength. The cylinders also had comparable strength with the exception of 40 mm diameter cylinder which showed 130 MPa strength due to its smallest size in the set. This strength variation in HSECC with specimen size is not in line with behaviour observed for normal concrete where the cubes tend to have greater strength than cylinders or prisms in compression. For normal concrete, the stress becomes concentrated along specimen's edge in case of cubes with lateral expansion being restraint by loading plate. Whereas the slender specimens also experience 'length effect' along with the stress concentration leading to greater decrease in the strength [36, 37]. However, this phenomenon is less pronounced in the context of HSECC due to the presence of a strong interfacial transition zone and a homogenous microstructure resulting from the incorporation of very fine aggregates (< 300 microns). It should further be noted that the effect of lateral expansion is more noticeable due to the difference in loading and placement direction [37]. This may be the reason of lesser strength in case of prism specimens. In general, it was observed that as the specimen size increased, the compressive strength decreased. This was due to the presence of smaller fracture process zone in small sized specimens which resulted in larger absorption capacity [38]. However, the difference was not as significant as typically observed in case of normal concrete.

Residual compressive strength

Specimens with square cross-section Figure 12 compares the normalised residual compressive strength of specimens with square cross section. The normalised compressive strength has been defined as the ratio of the compressive strength at a specific temperature to the average room temperature compressive strength. It can be observed that the residual strength varied with the size until 600 °C and became fairly similar at 800 °C. However, the exact trend of variation is not distinctly apparent due to a high deviation. Initial strength retention was in the range 86.4–98.8% at 200 °C with 100 mm cube showing the highest strength. On further increase in the temperature, the strength decreased as expected and this decrease was highest in 50 mm cube. This could be attributed to the 50 mm cube reaching the isothermal state faster than the other specimens, leading to higher initial decomposition in this temperature range.

In general, the effect of elevated temperature was less severe for larger sized specimens. This is likely because specimens with a higher volume-to-surface area ratio suffer less damage during initial heating stages due to the longer time required to reach the same temperature level. Notably, at 800 °C, the strength difference among various sized cubic specimens was minimal. This similarity suggests that at higher temperatures, the decomposition process reaches a near-completion stage, resulting in comparable phases of decomposition and consequently similar strength. CSH is transformed to C_2S and C_3S at this temperature potentially contributing to a degraded matrix [2] and hence, the strength

Fig. 12 Average residual compressive strength of specimens with square cross section
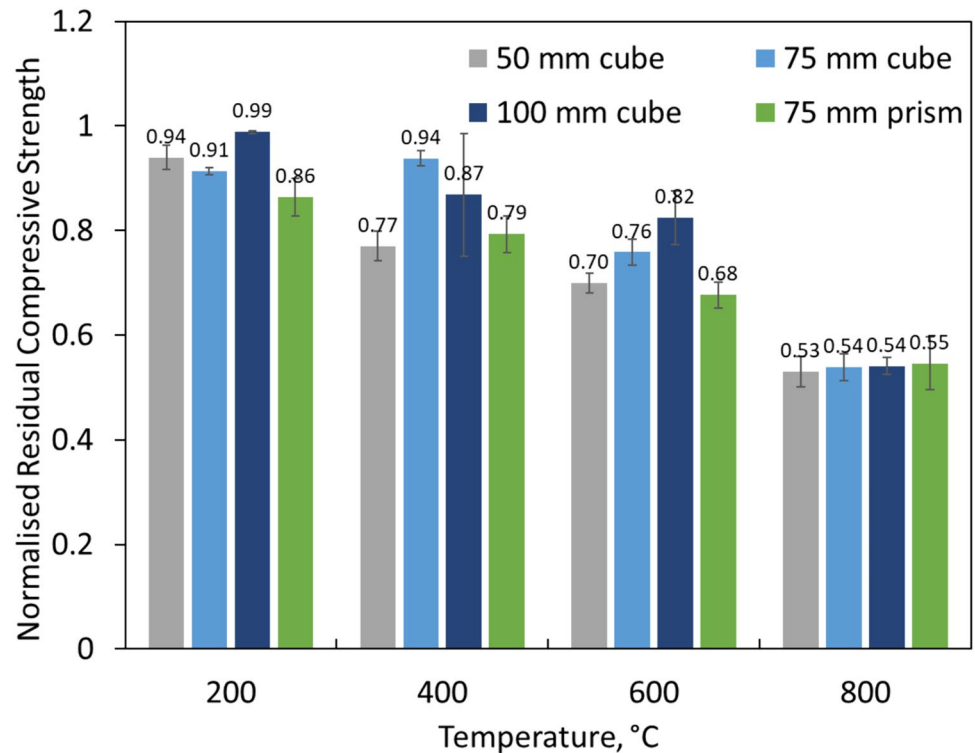
significantly decreased irrespective of the specimen size. Nonetheless, the specimen with higher volume and surface area may show different trend as further explained in the following section.

Interestingly, the overall trend is not in line with the rise in mass loss with specimen size (Fig. 7). This may have mainly been due to the dependency of the mass loss and compressive strength on different factors. Compressive strength at elevated temperatures is influenced by not only dehydration or evaporation of water, but decomposition and extent of microcracks may also significantly alter the strength. Therefore, unlike mass loss which mainly accounts for evaporation of water, the influence of degree and extent of temperature exposure will be more apparent for compressive strength. This was also confirmed by Yu et al. [35] who noted that the mass loss is affected with increase in duration of exposure only until 400 °C and thereafter, the effect of duration of exposure is minimal. However, the effect of duration was clearly noticeable for compressive strength at all temperature ranges. This observation is particularly crucial in the present case, as the time required to attain the isothermal state in different sized specimens will be different, affecting the degree to which specimens are heated.

The decrease in case of prism was also higher when compared with 75 mm cube as shown in Fig. 13. At a temperature of 600 °C, 75 mm cube exhibited around 75% strength retention, whereas the strength retention in case of prism was approximately 67%. The higher decrease may have been

mainly due to the larger height or surface area of the prism specimen directly exposed to the temperature, making it more susceptible to damage. This has also been previously highlighted by Zheng et al. [28] who inferred that the specimen with larger height suffer more damage. Moreover, a difference in the placement and loading direction as well as the lateral expansion due to size effect may have further amplified this effect. Nevertheless, as the temperature increased to 800 °C, the influence of size on the decomposition of hydration products diminished, resulting in approximately 60% strength retention. This may have again been due to the complete decomposition of hydration phases at this temperature as also evidenced in existing literature [2].

Specimens with circular cross-section Similar trend was observed for specimens with circular cross section as shown in Fig. 14 with distinctly evident size effect. With increase in the temperature, the specimens with lower size suffered higher increase; however, the difference tends to diminish at higher temperature range. This may have also been due to the lower volume (V) to surface area (SA) ratio of smaller sized specimens. At 200 °C, the lowest strength retention was seen in 40 mm cylinders (V/SA = 8) which retained around 84.6% strength, whereas the percentage retention was 91.6%, 93% and 95.17% for 75 mm diameter (V/SA = 15), 100 mm diameter (V/SA = 20) and 150 mm diameter cylinders (V/SA = 30) respectively. The same trend was observed with increase in temperature, the

Fig. 13 Comparison of average residual compressive strength between 75 mm cube and 75 mm prism
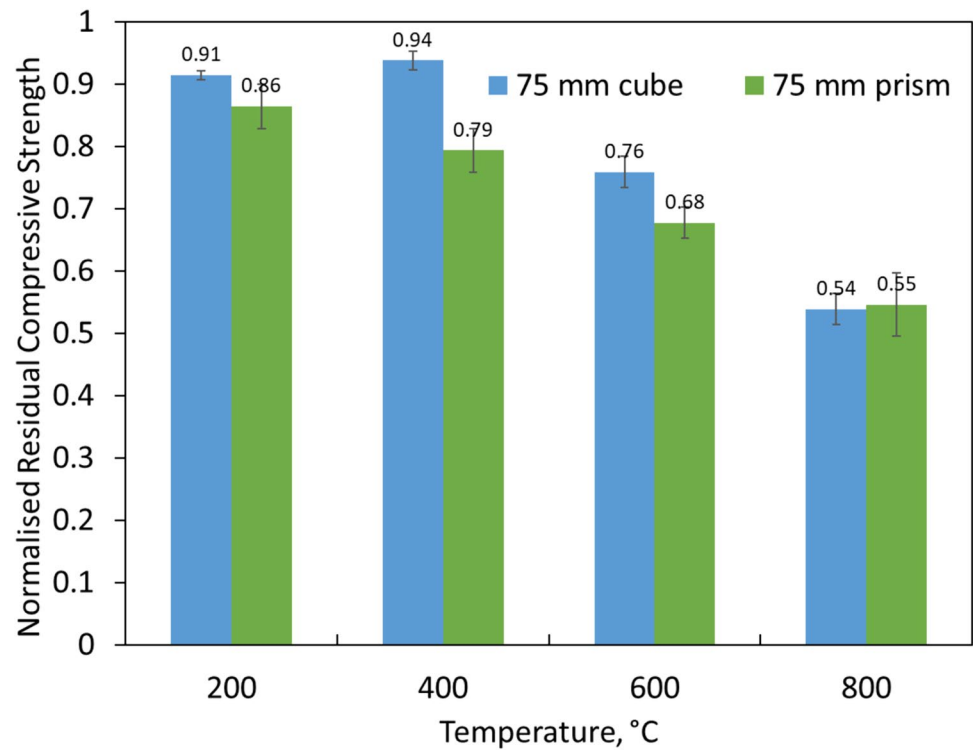
Fig. 14 Average residual compressive strength of specimens with circular cross section
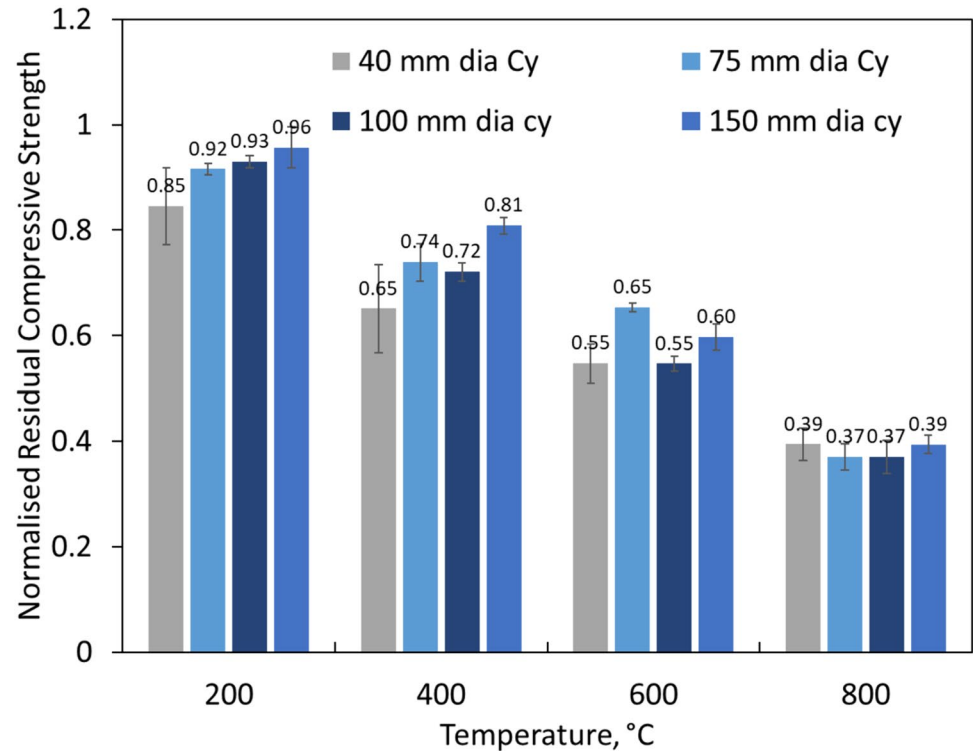
reason for the higher strength retention in 75 mm diameter cylinders at 600 °C is not clearly understood and warrants further investigation. At 800 °C, the effect of size of cylinders subsided and around 39% strength retention was observed for all specimen sizes. This suggests that at higher temperature range where the hydration products approach near complete decomposition stage, the influ-

ence of specimen size on strength may become insignificant.

The same reason could also be attributed to the greater strength reduction in case of 75 mm diameter cylinders compared to 75 mm prisms despite having the same aspect ratio as shown in Fig. 15. The reduction in strength was approximately 20% for 75 mm prisms, whereas 75 mm cylinder showed around 26% reduction at 400 °C. Since both 75 mm cylinder and prism have same volume to surface area ratio (V/SA = 15), a lesser decrease in case of prism could be related to its higher volume. Specimens with larger volumes are less susceptible to decomposition due to reduced exposure of their core at specific temperatures. Therefore, prisms experienced less strength reduction at elevated temperatures compared to cylinders, except at 200 °C. The strength loss below 400 °C is influenced by multitude of factors including fibre melting, pore-pressure dissipation, and the loss of chemically bound water. Additionally, there is a change in cohesion forces between the CSH layers which could have both positive or negative effect depending on the pozzolanic reactivity of the matrix constituents [39, 40]. Therefore, no distinct trend associated with size effect was observed in this temperature range and a detailed analysis of these observations may be required for establishing a clear trend at this temperature. Beyond 600 °C, the influence of these factors tends to diminish, especially since the fibres are nearly completely decomposed and the water is almost entirely evaporated and hence, a relatively consistent trend was observed.
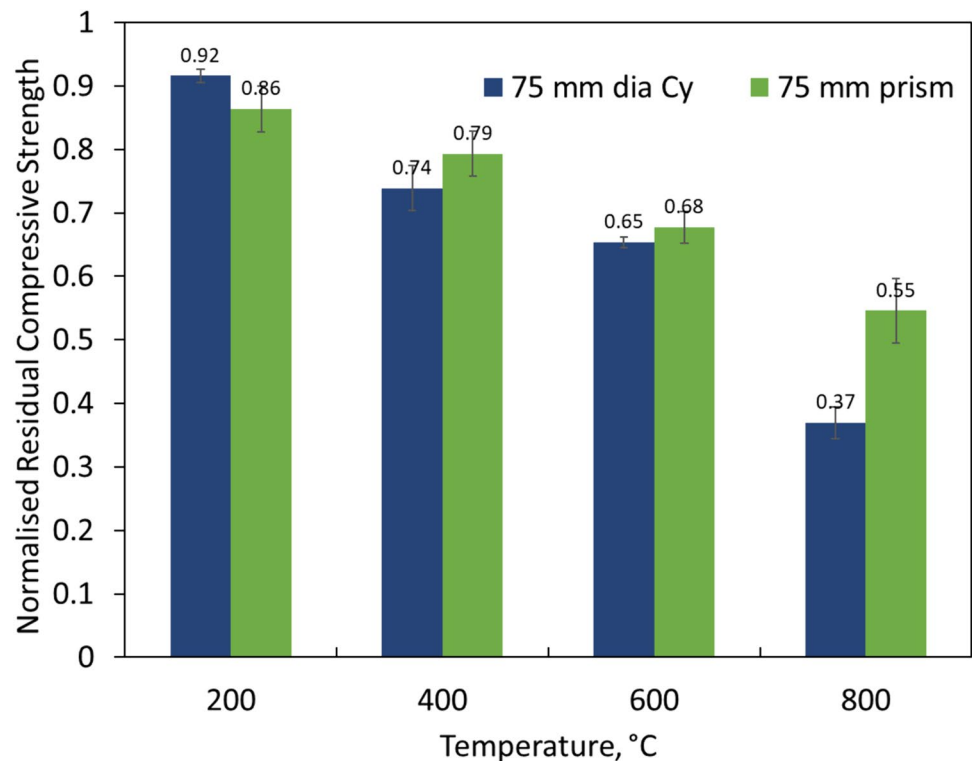
If the strength of specimens with different aspect and shape ratio is compared, the percentage decrease was observed to be higher in the specimens with higher aspect ratio. As shown in Fig. 16, cubic specimens suffered less decrease as compared to the cylinder specimens and the trend remained consistent from 200 to 800 °C. Considering the observed trend, surface area and volume to surface area ratio emerges as the primary parameter to consider. For the specimens with greater aspect ratio, the decrease will be generally higher due to their higher surface area directly exposed to heat load. For the specimens with roughly similar surface area, volume to surface area ratio could be used to define the variation trend with rise in temperature. It should further be noted the influence of specimen size may become less pronounced at higher temperatures, particularly at 800 °C, likely due to the decomposition that occurs. However, this effect also is contingent on the specimen type (cylinder vs. cube vs. prism) and how quickly the core reaches the specified temperature and the duration it remains at that temperature.

## Microstructural characterisation

SEM analysis

SEM analysis was performed to further compare the behaviour of different sized specimens. The analysis focused on the temperature range of 400–600 °C, where a consistent

Fig. 15 Comparison of average residual compressive strength between 75 mm cylinder and 75 mm prism

Fig. 16 Residual compressive strength of different sized HSECC specimens
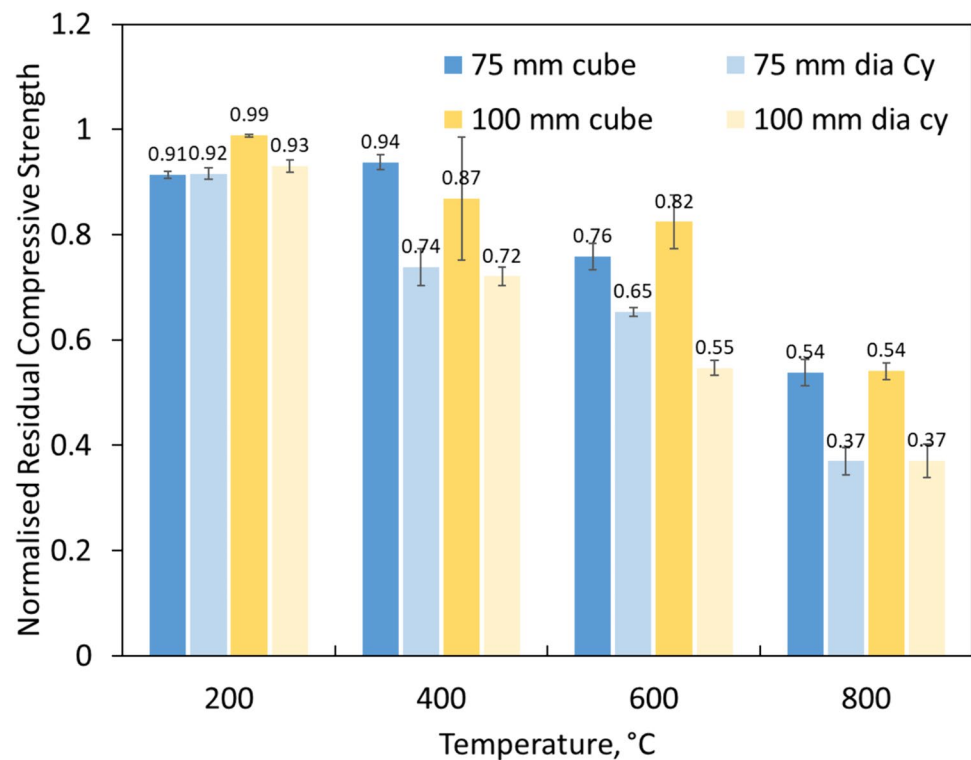
decomposition takes place, and the respective strength trend was also consistent. A comparison was made to distinctly assess the effect of specimen size (75 mm vs. 150 mm diameter cylinders) and specimen cross-section shape (75 mm cylinder and 75 mm prism).

Figure 17 shows the SEM micrographs of cylinder specimen with 75 mm and 150 mm diameter after exposure to 400 °C. It can be observed that the decomposition stage is almost similar in both specimens. Both micrographs exhibit compact microstructure with no observable degradation or microcracks. Furthermore, energy dispersive spectroscopy analysis confirmed the presence of the same types of elements in the analysed region, indicating that the dehydration or decomposition stage did not significantly differ between cylinders of different diameters. However, the difference in the residual strength might have occurred due to the varying relative quantity of different hydration compounds. As a result, phase analysis would be necessary to further understand this trend, which has been included in the subsequent section.

Figure 18 further shows the SEM micrographs of the specimen of different cross-sectional shape (75 mm prism and cylinder) after 600 °C exposure at two levels of magnification (1000× and 2500×). In both types of specimens, there were no observable microcracks near the molten fibre, and the decomposition stages of the material appeared similar. However, at 2500× magnification, microcracks were more evident in the cylinder samples compared to the prism

samples. These findings align with the results from compressive strength tests, which indicated that cylindrical samples exhibited lower strength retention. This provides further evidence that the presence of these microcracks likely contributed significantly to the observed differences between these specimens.

XRD analysis

Previous section examined how elevated temperatures affect microcrack formation in specimens of various sizes using SEM analysis. However, the influence of the size difference on decomposition processes could be better understood with XRD analysis. Figure 19 shows the X-ray diffraction curves of cylinder HSECC specimens after exposure to 400 and 600 °C, where major peaks of portlandite (18.04°, 34.11°, 47.13°, 64.28°), calcite (29.45°), ettringite (9.07°), albite (between 26.7–28°) and alite (31–33°) are highlighted. In addition, the peaks of quartz are also shown to establish a baseline for the relative comparison of different sized specimens.

The XRD results indicate that amount of ettringite is minimal in both specimens exposed to 400 and 600 °C, indicating that the decomposition had already initiated. Furthermore, as the temperature increases from 400 to 600 °C, the intensity of the portlandite peak decreases, also suggesting an ongoing decomposition process. Subsequently, at temperatures beyond 600 °C, the peaks

Fig. 17 SEM micrographs of **a** 75 mm **b** 150 mm diameter cylinder specimens after 400 °C exposure

(a) 75 mm cylinder

(b) 150 mm cylinder
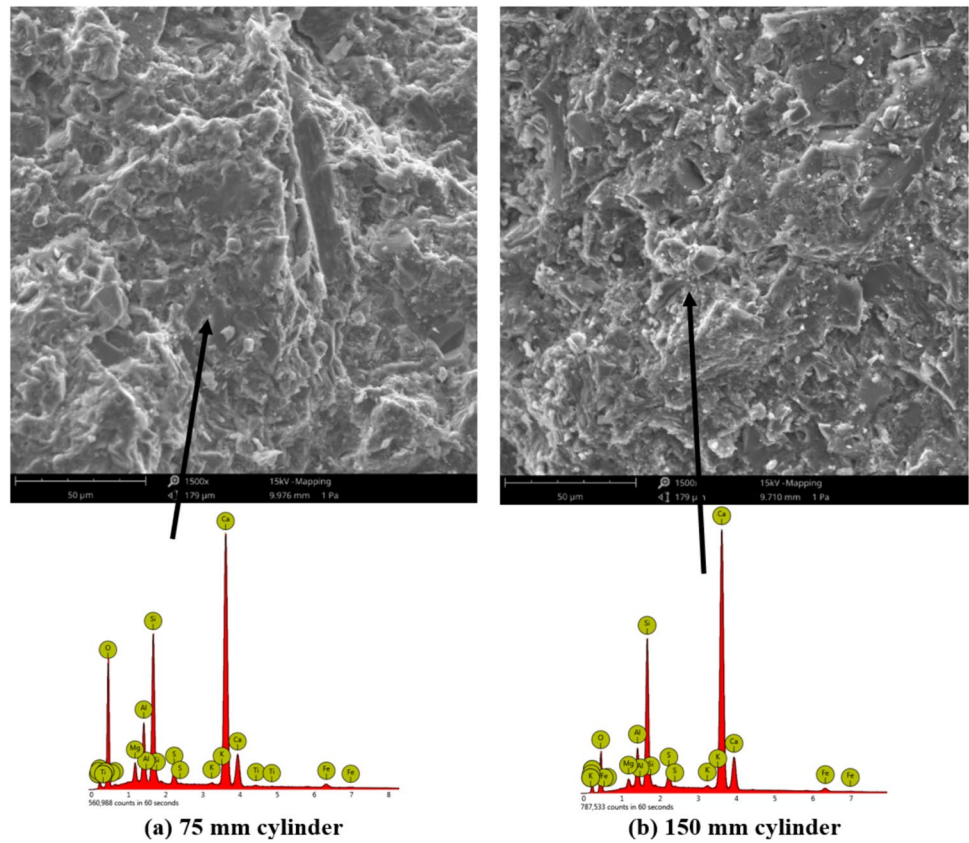
corresponding to calcite and other decomposed compounds become more pronounced. Additionally, a comparison can be further made among different cross-sectional area cylinders by comparing the major peak of portlandite at 18.04°. In specimens exposed to 400 °C (Fig. 19a), there is a noticeable increase in the intensity of this peak as the cylinder diameter increases from 40 to 150 mm, indicating a higher presence of hydration compounds. A similar trend is observed in specimens exposed to 600 °C (Fig. 19b). These findings are consistent with mechanical performance tests, which also indicate that larger specimens are less affected by elevated temperatures, possibly due to differences in the duration they remain at a specific temperature after reaching isothermal state.

If compared among the different shapes (75 mm prism, 75 mm cube vs. 75 mm cylinder), the peak phases and respective decomposition patterns was found to be almost identical (Fig. 20). There were no observable differences in the phases, indicating that the decomposition progresses at a similar rate for different specimen types. This finding suggests that altering the shape of the specimen might not significantly impact the decomposition pattern when exposed to high temperatures. However, the extent of microcracks may vary as observed through SEM analysis and this may have resulted into the slight variation in the strength.

Conclusions

This study investigated the influence of size of HSECC specimens on the compressive performance after exposure to temperatures from 200 to 800 °C. Cylinder specimens with 40–150 mm diameter (height/diameter = 2:1), cubes with size 50–100 mm side and prism of size $75 \times 75 \times 150$ mm were selected to study the effect of specimen size and shape on the residual compressive strength. Based on the observations, the following conclusions can be drawn:

- Specimen size did not have significant influence on mass loss especially for temperature above 400 °C. A slight variation was observed at 200 °C which could be attributed to the higher mass loss caused by prolonged exposure duration. However, residual compressive strength was found to be considerably influenced by both specimen size and shape. This was in clear contradiction to the existing study [8] that had indicated no significant impact of size on strength under high temperature exposure. Nevertheless, this difference diminishes at higher temperature ranges, particularly beyond 600 °C.
- The obtained results suggested a strong correlation between the residual strength and aspect ratio or the volume to surface area of specimens. In general, the cubic specimens (aspect ratio 1) suffered less strength loss for

Fig. 18 SEM micrographs of specimens with 75 mm cross-section **a** cylinder **b** prism after 600 °C exposure (×1000, ×2500 magnification)

(a) 75 mm cylinder   (b) 75 mm prism
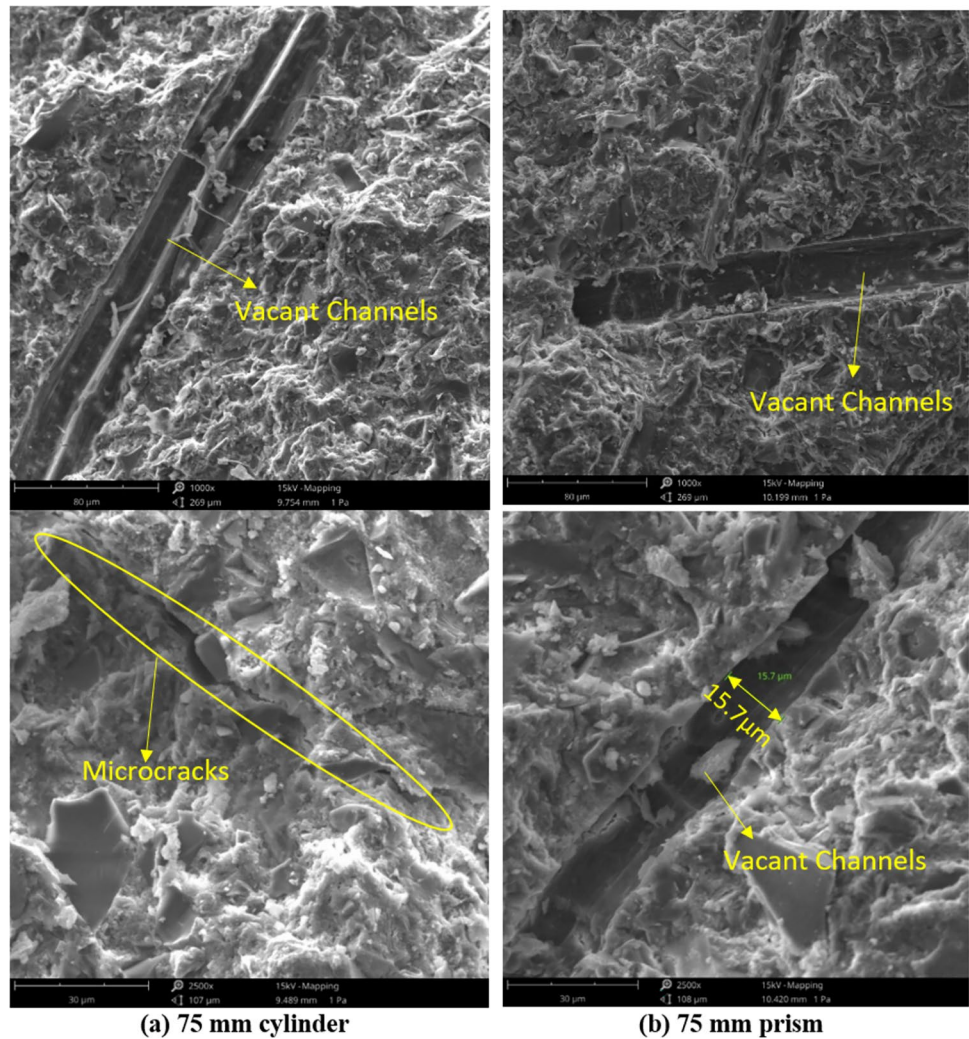
the same cross-section sized prisms (aspect ratio 2). It was also noted that specimens with lower volume-to-surface-area (at constant aspect ratio) deteriorated more rapidly due to faster heating at a specific temperature.

- Based on the consistency of results and optimal utilization of material, the use of 75–100 mm diameter cylinder specimens (with 2-hour exposure duration) is recommended for elevated temperature studies on HSECC. Adoption of this size would ensure coherent results with minimal influence of external factors such as fibre melt-

ing, placement direction or heightened exposure which are critical below 400 °C.

- While specimen type clearly influenced compressive strength variations, establishing a definitive relationship between specimen size or shape and resulting residual compressive strength may require further experimental trials, considering time to reach the isothermal stage and varying heating rates. Future studies should explore precise dwell durations based on isothermal stages for specimens of different sizes to establish clearer trends.

Fig. 19 X-ray diffractograms of cylinder specimens at temperature exposure of **a** 400 °C **b** 600 °C [A—Alite, A′—Albite, C—Calcite, E—Ettringite, P—Portlandite, Q—Quartz]
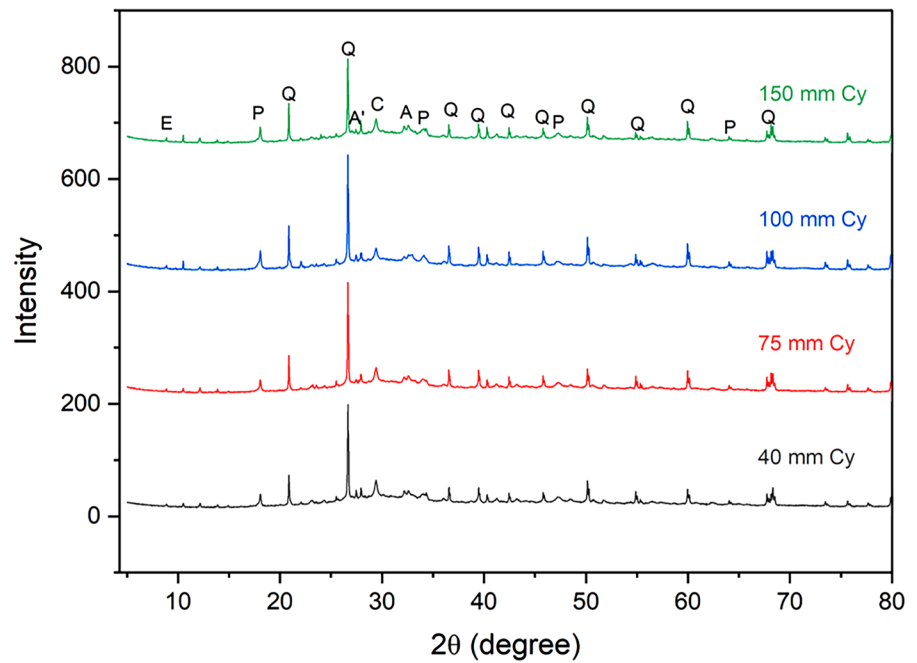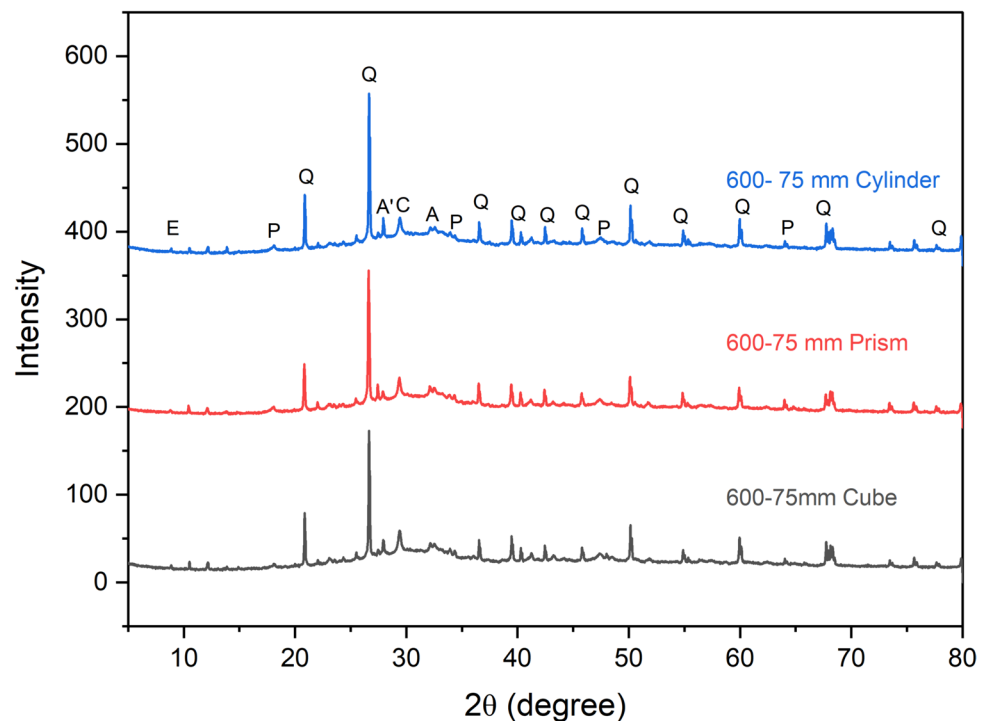

(a) 400°C
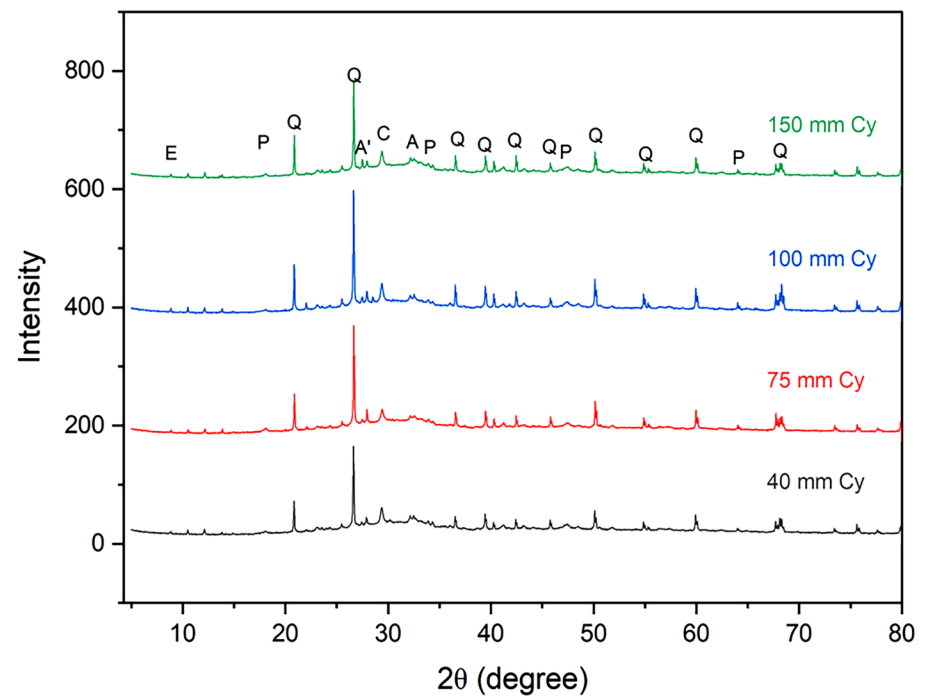
(b) 600°C

Fig. 20 X-ray diffractograms of specimens with 75 mm cross-section after 600 °C exposure [A—Alite, A′—Albite, C—Calcite, E—Ettringite, P—Portlandite, Q—Quartz]

Declarations

Conflict of interest The authors declare that they have no known conflict of interests or personal relationships that could have appeared to influence the work reported in this paper.

References

1. Pourfalah S (2018) Behaviour of engineered cementitious composites and hybrid engineered cementitious composites at high temperatures. Constr Build Mater 158:921–937
2. Rawat S, Lee CK, Zhang YX (2021) Performance of fibre-reinforced cementitious composites at elevated temperatures: a review. Constr Build Mater 292:123382
3. Erdem TK (2014) Specimen size effect on the residual properties of engineered cementitious composites subjected to high temperatures. Cem Concr Compos 45:1–8
4. Fanella D, Krajcinovic D (1988) Size effect in concrete. J Eng Mech 114(4):704–715
5. Li L, Gao D, Li Z, Cao M, Gao J, Zhang Z (2020) Effect of high temperature on morphologies of fibers and mechanical properties of multi-scale fiber reinforced cement-based composites. Constr Build Mater 261:120487
6. Rawat S, Zhang YX, Lee CK (2023) Spalling resistance of hybrid polyethylene and steel fiber-reinforced high-strength engineered cementitious composite. In: Duan W, Zhang L, Shah SP (eds) Nanotechnology in construction for circular economy. NICOM 2022. Lecture notes in civil engineering, vol 356. Springer, Singapore
7. Hilal N, Saleh RD, Yakoob NB, Banyhussan QS (2021) Utilization of ceramic waste powder in cement mortar exposed to elevated temperature. Innov Infrastruct Solut 6(1):35
8. Li Y, Yang EH, Tan KH (2019) Effects of heating followed by water quenching on strength and microstructure of ultra-high performance concrete. Constr Build Mater 207:403–411
9. Nodehi M, Gencel O, Erdogmus E, Karagöz ME, Shi J, Mo KH, Gholampour A, Ozbakkaloglu T (2024) Effect of cement type and water-to-cement (w/c) ratio on characteristics of lightweight mortars produced with pumice: a comparative study on calcium aluminate (rapid hardening) and ordinary Portland cements. Innov Infrastruct Solut 9(2):1–23

10. Zhang D, Liu Y, Tan KH (2021) Spalling resistance and mechanical properties of strain-hardening ultra-high performance concrete at elevated temperature. Constr Build Mater 266:120961

11. Zhang P, Han Q, Wu J, Zhang Y, Zhang T (2022) Mechanical properties of nano-SiO_2 reinforced engineered cementitious composites after exposure to high temperatures. Constr Build Mater 356:129123

12. Zhang X, Lyu X, Zhang X, Lou C (2024) Effect of high temperature on mechanical properties of polyethylene fibre-calcium carbonate whisker engineered cementitious composites. Dev Built Environ 18:100462

13. Lu L, Han F, Wu S, Qin Y, Yuan G, Doh J-H (2022) Experimental study on durability of basalt fiber concrete after elevated temperature. Struct Concr 23:682–693

14. He J, Wang Q, Yao B, Ho J (2021) Impact of elevated temperatures on the performance of high-strength engineered cementitious composite. J Mater Civ Eng 33(9):04021222

15. Wang Q, Zhou Y, Lai M, Gu M, Ho JCM (2023) Carbon fiber to improve the resistance of high strength PVA-ECC to elevated temperatures. J Build Eng 71:106475

16. Baskara Sundararaj J, Kannan Rajkumar PR, Sivasakthi M, Jegan M (2022) Effect of mineral admixtures on mechanical and thermal properties of geopolymer mortar at elevated temperature. Innov Infrastruct Solut 7(6):354

17. Chen J, Zhu Z, Zhou L, Zhuang J, Wang M, Ma L (2023) Study on mechanical properties of (1% PVA fiber + 1% steel fiber) PS-ECC under the coupling effects of elevated temperature and dynamic loads. Struct Concr. https://doi.org/10.1002/suco.202200070

18. Deshpande AA, Kumar D, Ranade R (2019) Influence of high temperatures on the residual mechanical properties of a hybrid fiber-reinforced strain-hardening cementitious composite. Constr Build Mater 208:283–295

19. Tangirala A, Rawat S, Lahoti M (2023) High volume fly ash and basalt-polypropylene fibres as performance enhancers of novel fire-resistant fibre reinforced cementitious composites. J Build Eng 107586

20. Rawat S, Zhang YX, Fanna DJ, Lee CK (2024) Development of sustainable engineered cementitious composite with enhanced compressive performance at elevated temperatures using high volume GGBFS. J Clean Prod 451:142011

21. Yoo DY, Kim S, Park GJ, Park JJ (2020) Residual performance of HPFRCC exposed to fire-effects of matrix strength, synthetic fiber, and fire duration. Constr Build Mater 241:118038

22. Dabbaghi F, Dehestani M, Yousefpour H (2022) Residual mechanical properties of concrete containing lightweight expanded clay aggregate (LECA) after exposure to elevated temperatures. Struct Concr 23(4):2162–2184

23. Chen M, Wang Y, Zhang T, Zhang m (2023) Microstructural evolution and dynamic compressive properties of engineered cementitious composites at elevated temperatures. J Building Eng 71:106519

24. Tanyildizi H, Bulut M (2024) Self-healing performance of nano-silica-modified engineered cementitious composites exposed to high temperatures. J Mater Civ Eng 36(6):04024109

25. Tang J, Ma W, Pang Y, Fan J, Liu D, Zhao L, Sheikh SA (2021) Uniaxial compression performance and stress–strain constitutive model of the aluminate cement-based UHPC after high temperature. Constr Build Mater 309:125173

26. Li QH, Sun CJ, Xu SL (2019) Thermal and mechanical properties of ultrahigh toughness cementitious composite with hybrid PVA and steel fibers at elevated temperatures. Compos Part B: Eng 176:107201

27. Zhang P, Han X, Hu S, Wang J, Wang T (2022) High-temperature behavior of polyvinyl alcohol fiber-reinforced metakaolin/fly ash-based geopolymer mortar. Compos Part B: Eng 244:110171

28. Zheng W, Luo B, Wang Y (2013) Compressive and tensile properties of reactive powder concrete with steel fibres at elevated temperatures. Constr Build Mater 41:844–851

29. Zheng W, Luo B, Wang Y (2014) Microstructure and mechanical properties of RPC containing PP fibres at elevated temperatures. Mag Concr Res 66(8):397–408

30. Bamonte P, Gambarova PG (2010) Thermal and mechanical properties at high temperature of a very high-strength durable concrete. J Mater Civ Eng 22(6):545–555

31. Akca AH, Zihnioğlu NÖ (2013) High performance concrete under elevated temperatures. Constr Build Mater 44:317–328

32. Rawat S, Lee CK, Zhang YX (2024) Green engineered cementitious composites with enhanced tensile and flexural properties at elevated temperatures. Clean Mater 12:100240

33. Rashad AM, Morsy MS, El-Nouhy HA (2009) Effect of elevated temperature on physico-mechanical properties of metakaolin blended cement mortar. Struct Eng Mech 31(1):1–10

34. Morsy MS, Rashad AM, Shebl SS (2008) Effect of elevated temperature on compressive strength of blended cement mortar. Build Res J 56(2–3):173–185

35. Yu KQ, Dai JG, Lu ZD, Leung CK (2015) Mechanical properties of engineered cementitious composites subjected to elevated temperatures. J Mater Civ Eng 27(10):04014268

36. Kim JK, Yi ST, Kim JHJ (2001) Effect of specimen sizes on flexural compressive strength of concrete. ACI Struct J 98(3):416–424

37. Yi ST, Yang EI, Choi JC (2006) Effect of specimen sizes, specimen shapes, and placement directions on compressive strength of concrete. Nucl Eng Des 236(2):115–127

38. Fládr J, Bílý P (2018) Specimen size effect on compressive and flexural strength of high-strength fibre-reinforced concrete containing coarse aggregate. Compos Part B: Eng 138:77–86

39. Seleem HEH, Rashad AM, Elsokary T (2011) Effect of elevated temperature on physico-mechanical properties of blended cement concrete. Constr Build Mater 25(2):1009–1017

40. Dawood ET, Alattar AA, Abbas WA, Mohammad YZ (2020) Behavior of foamed concrete reinforced with hybrid fibers and exposed to elevated temperatures. SN Appl Sci 2(1):84